2013 American Control Conference (ACC)
Washington, DC, USA, June 17-19, 2013

Multimode and multitone analysis of the dynamic mode operation of the Atomic Force Microscope

Govind Saraswat, Pranav Agarwal and Murti V. Salapaka

Abstract— **This article investigates the multimode model of the cantilever beam during probe based imaging. It develops a framework to quantify the effects of different material properties like dissipativity and stiffness in a near tapping mode operation of Atomic Force Microscope (AFM), which is the primary mode of imaging soft matter, when excitation consists of more than one sinusoids. Averaging theory forms an important basis and provides the theoretical foundations. Effect of dissipative and stiffness properties of the sample on the forces experienced by probe is modeled as changes in parameters of an equivalent linear time invariant model, of the cantilever-sample system. It is shown that this model can be extended to the case when multiple modes of the cantilever participate in the nonlinear interaction with the sample forces.**

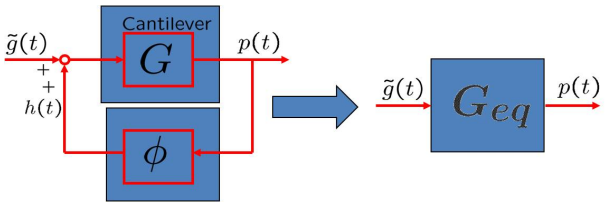

Fig. 1. Figure shows that using averaging theory, the cantilever being forced by $\tilde{g}(t)$ and the tip-sample separation dependent force ϕ with the tip deflection $p(t)$ can be viewed as an equivalent cantilever with changed resonant frequency ω_e and quality factor Q_e being forced by $\tilde{g}(t)$ resulting in the deflection $p(t)$ (with no sample force ϕ.)

I. INTRODUCTION

Cantilever probe based interrogation systems have revolutionized nanoscale investigation and design of material [1]. AFMs fall within this class of systems where a cantilever beam with a sharp tip at one end is employed to probe material with sub-nanometer resolution. Most of the methods and analysis used in the past were based on the single-mode approximation of the cantilever beam but recently, newer modalities of operation are employing higher modes of the cantilever flexure beam and are also using novel means of excitation. In the most commonly used mode of operation, the dynamic mode, also called the tapping mode, the cantilever is excited either at the base or at the other end, inducing oscillations in the cantilever. A single mode model is commonly used in this case to approximate the cantilever dynamics. Typically, the excitation is at, or near, the first modal frequency of the cantilever and the amplitude and phase of the cantilever oscillations at the forcing frequency are used to image the topography. In standard operation, the amplitude is regulated at a desired set-point and the control signal used to regulate the amplitude provides an image of the sample topography. Here,the cantilever-sample system can be represented by a Lur'e system as described in Fig. 1 where G represents the cantilever model, a linear-time-invariant system, ϕ represents a static nonlinearity that characterizes the force exerted by the sample on the cantilever which depends on the tip-sample separation, and the exogenous forcing is shown by $\tilde{g}$.

By using the tools of averaging theory, the cantilever-sample system (which is nonlinear and time varying) under the sinusoidal forcing can be imagined to be an equivalent linear time-invariant (LTI), spring-mass-damper system with changed resonant frequency and damping factors (see Fig.1). There is an evolving knowhow of these equivalent cantilever parameters relations to local sample dissipativity and sample stiffness[2]. The understanding of these concepts in the multi-mode case is scant. However, even in the standard one mode approximation, there are no real-time methods to identify these equivalent parameters other than the preliminary result reported by the authors (see [3]). In [3], to ascertain the robust estimation of these parameters, the cantilever was forced at a multitone input formed by a sum of three sinusoids. The results in [3] assumed the equivalent parameters which are arrived at assuming a single tone excitation. There is thus a need to evaluate the effect of a multi-tone excitation on the parameters of the equivalent LTI model that approximates the behavior of the cantilever-sample interconnection where the forcing $\tilde{g}$ is a sum of sinusoids. In this article we first apply averaging theory to arrive at a linear time invariant model for a one mode approximation of the cantilever interacting with the sample while being forced by a sum of sinusoids. Furthermore relations that connect parameters of the LTI model to the sample stiffness and dissipation are derived.

In the second part of the article a multi-mode approximation of the cantilever dynamics is emphasized. Main motivations for employing a multimode description of the cantilever dynamics is based on recent discoveries that indicate that multiple modes of the cantilever do get excited while imaging. This has also led to a slew of new methods which include strategies where information is gathered passively by monitoring the second mode while the cantilever is excited at the first modal frequency (see [4] and [5]) and strategies where the second mode is intentionally forced together with the first mode [6]. Even though these new modes of dynamic mode imaging show clear advantages, the understanding of why and when these advantages accrue is scant. Indeed most of the advantages are inferred from the *contrast* observed in images as the cantilever scans over

978-1-4799-0178-4/$31.00 ©2013 AACC

different material; what the contributing factors are to the contrast and what it entails is not well understood (see also [6] for a similar assessment). In this paper, we develop a framework to analyze and understand the dynamic mode operation for discerning sample properties under multi-tone excitation and multi-mode approximation. Simulation results on a model that closely follows the physics corroborate the theoretical analysis.

The paper is organized as follows. In Section II the equivalent cantilever model under single mode approximation is developed and applicability of averaging theory to a multi-tone input is analyzed ; in Section III similar concepts are extended to a multimode model while Section IV summarizes the main points and gives future direction.

II. Equivalent Cantilever Model

Envisioning the cantilever-sample system as an equivalent cantilever is the process of arriving at a linear time-invariant model (the equivalent cantilever) of a nonlinear time-varying system (the cantilever together with the tip-sample interactions). The $G-\phi$ interconnection (Fig.1), with a one mode approximation of the cantilever dynamics, can be written as

$$m\ddot{p}+\tilde{c}\dot{p}+kp=\tilde{\phi}(p,\dot{p})+m\tilde{g}(t) \tag{1}$$

where $p(t)$ is the instantaneous cantilever position, k is the spring constant, $\tilde{c}$ is the damping coefficient, $\tilde{g}(t)$ is the dither excitation and $\tilde{\phi}(p,\dot{p})$ is the force due to nonlinear tip-sample interaction. Let $\omega^2=k/m$ be the resonant frequency. Assuming that the damping $\tilde{c}$, forcing $\tilde{g}$, and the tip-sample interaction $\tilde{\phi}$ are small we define $\tilde{c}=\varepsilon c$, $\tilde{g}=\varepsilon g$, and $\tilde{\phi}=\varepsilon\phi$, where, ε is a small parameter (which is the case for typical cantilever used with AFM). It follows from (1) that

$$\ddot{p}+\omega^2 p=(\varepsilon/m)\phi(p,\dot{p})+(\varepsilon/m)g(t)-(\varepsilon/m)c\dot{p} \tag{2}$$

Consider a change of coordinates, $(p,\dot{p})\rightarrow(a,\theta)$ via

$$p=a\cos(\omega t+\theta);\ \ \dot{p}=-a\omega\sin(\omega t+\theta). \tag{3}$$

Differentiating the relations in (3) with respect to time, we obtain the dynamics in the changed coordinates as

$$\begin{aligned}\dot{a} &= -\tfrac{\varepsilon}{\omega m}[\phi(a\cos(\omega t+\theta),-a\omega\sin(\omega t+\theta))+\\ &\quad c(a\omega\sin(\omega t+\theta))+g(t)]\sin(\omega t+\theta)\end{aligned} \tag{4}$$

$$\begin{aligned}\dot{\theta} &= -\tfrac{\varepsilon}{\omega m}[\phi(a\cos(\omega t+\theta),-a\omega\sin(\omega t+\theta))\\ &\quad +c(a\omega\sin(\omega t+\theta))+g(t)]\cos(\omega t+\theta).\end{aligned} \tag{5}$$

In the case of monotone excitation ($\tilde{g}(t)=E\sin\omega t$), the dynamics (4) and (5) are periodic with period $\frac{2\pi}{\omega}$. In [2], authors exploit the periodic nature of the (a,θ) dynamics, and used averaging theory [7] to convert the non-autonomous dynamics given by (4) and (5) to an autonomous system. The first order periodic averaging [8] theorem states that

Theorem II.1 (First order periodic averaging). *Consider*

$$\begin{aligned}\dot{x}&=\varepsilon f(t,x); \qquad x(0)=x_0;\ \textit{and}\\ \dot{x}_{av}&=\varepsilon f_{av}(x_{av}); \quad x_{av}(0)=x_0\end{aligned} \tag{6}$$

where $f(t,x)$ is T periodic function in the variable t and $f_{av}(x):=\frac{1}{T}\int_0^T f(\tau,x)d\tau$. Then with mild assumptions on f, there exist constants L and M such that

$sup_{t\in[0,\frac{L}{\varepsilon}]}|x(t)-x_{av}(t)|\leq M\varepsilon.$

Application of Theorem II.1 to the nonlinear time varying dynamics (4) and (5) results in the averaged time-invariant dynamics as described below (where with some abuse of notation we represent the averaged amplitude and phase by a and θ only).

$$\begin{aligned}\dot{a} &= -\tfrac{c_e(a)}{2m}a-\tfrac{\varepsilon}{2m\omega}E\sin\theta,\\ \dot{\theta} &= \omega_e(a)-\omega-\tfrac{\varepsilon}{2ma\omega}E\cos\theta,\ \text{where}\end{aligned} \tag{7}$$

$$\omega_e^2(a) = \omega^2-\frac{2}{am}\overline{\Phi}_c; \tag{8}$$

$$\frac{c_e(a)}{2m} = \frac{\tilde{c}}{2m}+\frac{1}{am\omega}\overline{\Phi}_d \tag{9}$$

with $\overline{\Phi}_c=\frac{1}{2\pi}\int_0^{2\pi}\tilde{\phi}(a\cos\psi,-a\omega\sin\psi)\cos\psi d\psi$ and $\overline{\Phi}_d=\frac{1}{2\pi}\int_0^{2\pi}\tilde{\phi}(a\cos\psi,-a\omega\sin\psi)\sin\psi d\psi$. We can revert the averaged dynamics in the (a,θ) coordinates to the original $(p,\dot{p})$ coordinates. It can be shown, by using the relations $p=a\cos(\omega t+\theta)$ and $\dot{p}=-a\omega\sin(\omega t+\theta)$ where a and θ evolve according the averaged dynamics (7) that

$$\ddot{p}+\frac{c_e(a)}{m}\dot{p}+\omega_e(a)^2p=\frac{1}{m}\tilde{g}(t) \tag{10}$$

The above dynamics describes an *equivalent cantilever* with changed resonant frequency ω_e and damping c_e being forced by the excitation $\tilde{g}(t)$. We remark that the equivalent damping c_e and the equivalent stiffness $k_e:=m\omega_e^2$, depend on the instantaneous amplitude a of the cantilever which varies with time. However, the amplitude is a slow varying parameter and in the time-scale of interest, the amplitude can be considered a constant. It follows from equations (8) and (9), that the change in the stiffness and damping coefficient are given by $-\frac{2}{a}\overline{\Phi}_c$ and $\frac{1}{a\omega}\overline{\Phi}_d$ respectively. Fig.2 shows simulation results that provide strong corroboration that the

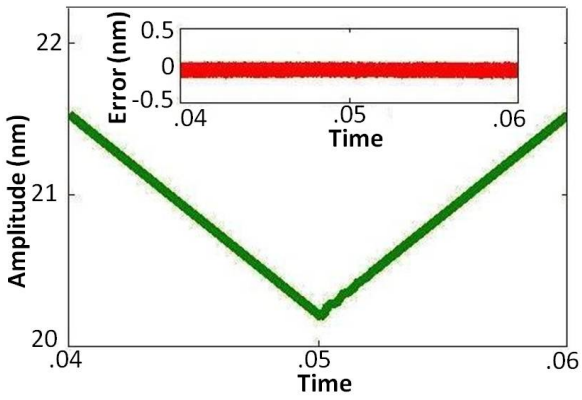

Fig. 2. Shows the amplitude of the first harmonic. In the approach phase(from 0.04s to 0.05s) the amplitude reduces from 21.5nm to 20.2nm and in the retract phase the amplitude recovers to 21.5nm. The amplitude as obtained by the averaged dynamics closely follows the original amplitude shown; inset shows the error to be within $\pm 0.1nm$

amplitude trajectories of the averaged dynamics (7) provide a good approximation to that of the original dynamics (4) and (5).

A. Deriving Sample Properties from Equivalent Cantilever Parameters

It is evident that from the knowledge of the nominal parameters (k, $\tilde{c}$ and ω), the equivalent cantilever parameters (k_e and c_e), and the amplitude a, it is possible to determine $\overline{\Phi}_c$ and $\overline{\Phi}_d$ (see (8) ,(9)). As $\overline{\Phi}_d$ characterizes the difference between the equivalent damping and nominal damping and $\overline{\Phi}_c$ characterizes the difference between the equivalent resonant frequency and nominal resonant frequency, we can view $\overline{\Phi}_d$ and $\overline{\Phi}_c$ as the dissipative and conservative properties of the sample respectively. Indeed it can be shown that within $\mathscr{O}(\varepsilon)$

$$-\frac{1}{T}\int_0^T \phi(p,\dot{p})\dot{p}dt = \frac{1}{T}\int_0^T (c_e-\tilde{c})\dot{p}^2 dt = a\omega\overline{\Phi}_d \qquad (11)$$

where $-\frac{1}{T}\int_0^T \phi(p,\dot{p})\dot{p}dt =: \overline{\Phi}_D$ denotes the power dissipated by the sample whereas $\frac{1}{T}\int_0^T (c_e-\tilde{c})\dot{p}^2 dt$ denotes the power lost by a viscous damper in a spring-mass-damper system with damping coefficient $(c_e-\tilde{c})$. Thus the power lost to the sample is equal to the power lost by an equivalent viscous damper with coefficient $c_e-\tilde{c}$. This further bolsters the equivalent cantilever description. It immediately follows from this discussion that if the sample is conservative then $\overline{\Phi}_d = 0$. A similar interpretation hold for $\overline{\Phi}_c$ (see [7]) where the notion of reactive power in electrical circuits is generalized to mechanical systems and it can be shown that $\overline{\Phi}_c$ represents the reactive power. Thus the change in the stiffness parameter characterizes the reactive power (which is non-dissipative) of the sample.

B. Recursive Estimation of Equivalent Cantilever Parameters (REEP)

We see that the equivalent cantilever parameters depend on slowly varying amplitude a. It follows that if the estimation scheme is fast compared to the evolution of the amplitude dynamics, then the dynamics described by (10) is a linear time-invariant system in the estimation time scale. Thus the problem of estimating equivalent cantilever parameters is transformed to identification of a linear time-invariant system (10). [3] has reported a method (the REEP algorithm) for recursively estimating the parameters (k_e and c_e) of the equivalent cantilever which adaptively estimates coefficients of the second order system (10). Consider Equations (8) and (9) that relate the equivalent parameters, the nominal parameters and $\bar{\Phi}_c$ and $\bar{\Phi}_d$. In these equations, c_e and ω_e are estimated in real-time, the nominal cantilever parameters are known and therefore, $\bar{\Phi}_c$ and $\bar{\Phi}_d$, which characterize the sample's reactive power and dissipative power respectively can be determined in real-time.

REEP algorithm formulates the estimation of equivalent parameters as that of solving a recursive least square problem. It was observed experimentally and through simulations ([3]) that with mono-frequency excitation $\tilde{g}(t) = E\sin\omega t$ it was not possible to estimate the parameters of the second order system (10) within the desired times scales. It was concluded that multi-frequency forcing will make the estimation process more robust and faster. This led to the excitation signal of the form $\tilde{g} = \gamma\sin(\omega t) + \gamma_+\sin(\omega + \Delta\omega)t + \gamma_-\sin(\omega-\Delta\omega)t$ The magnitudes γ_+ and γ_- and the sideband frequencies $(\omega \pm \Delta\omega)$ were chosen to ensure that the trajectory of the cantilever is minimally altered when compared to the single frequency excitation while facilitating robustness in parameter estimation. The need for $\tilde{g}$ to be richer than a single sinusoid implies that it is difficult to have $\tilde{g}$ to be periodic leaving Theorem II.1 no longer applicable. Thus, the validity of the equivalent cantilever approximation has to be analyzed under the new excitation that has multitones. We next develop the equivalent cantilever model for the multitone case.

C. Multitone Excitation

By using tools from [8], we derive equivalent cantilever concept for multitone excitation. The result is summarized in the theorem below and a sketch of the proof follows.

Theorem II.2. *Consider the dynamic system given by (2) with forcing $\tilde{g}(t) = A\sin\gamma t + B_1\sin(\gamma-\alpha)t + B_2\sin(\gamma+\alpha)t$ where γ is such that*

$$\varepsilon\Delta = \gamma^2 - \omega^2$$

with $\alpha = \mathscr{O}(\varepsilon)$. Then the system can be approximated by that of a linear system with equivalent damping coefficient $c_e(a)$ and equivalent resonant frequency $\omega_e(a)$ (as in (10)) forced by a input of form $\tilde{g}(t)$ with error of $\mathscr{O}(\varepsilon)$ on the time scale $1/\varepsilon$.

In the derivation of the theorem, we again do a change of coordinates via (3), and after some trigonometric manipulations, we get

$$\begin{pmatrix} \dot{a} \\ \dot{\theta} \end{pmatrix} = -\varepsilon F(a,\theta,t,\alpha t) \qquad (12)$$

where F is a sum of finite periodic vector fields. Let us introduce the new independent variable $\tau = \alpha t$, then the system can be written as

$$\begin{aligned} \begin{pmatrix} \dot{a} \\ \dot{\theta} \end{pmatrix} &= -\varepsilon F(a,\theta,t,\tau) \\ \dot{\tau} &= \alpha \end{aligned} \qquad (13)$$

with appropriate initial conditions. With τ an independent variable, F can be shown to be periodic over $2\pi/\gamma$. Thus, we can average the system over t keeping τ constant, which gives the averaged equations

$$\begin{aligned} \begin{pmatrix} \dot{a_{av}} \\ \dot{\theta_{av}} \end{pmatrix} &= -\varepsilon F^0(a_{av},\theta_{av},t,\tau_{av}) \\ \dot{\tau_{av}} &= \alpha \end{aligned} \qquad (14)$$

or

$$\begin{pmatrix} \dot{a_{av}} \\ \dot{\theta_{av}} \end{pmatrix} = -\varepsilon F^0(a_{av},\theta_{av},t,\alpha t) \qquad (15)$$

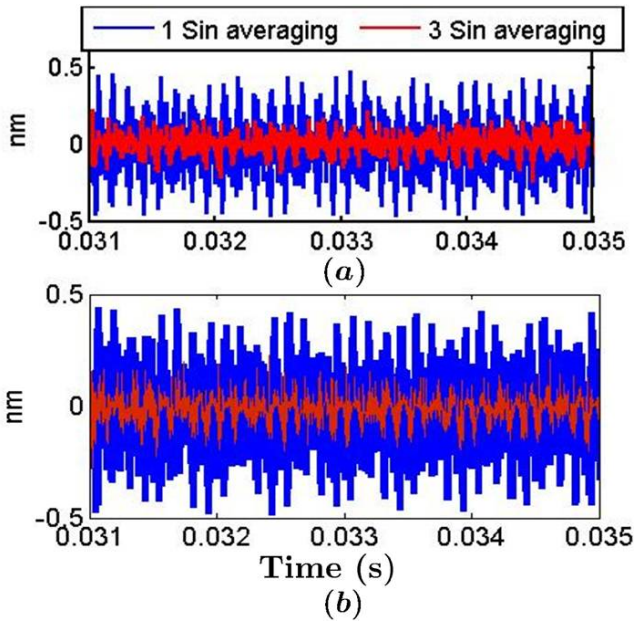

Fig. 3. Simulation results for difference in steady state trajectories of actual simulation with Monotone averaged equations and Averaged Equations with multitone excitation for α = 8kHz and a step input of (a)1nm and (b)2nm. Clearly multitone averaging is able to better approximate the trajectories

where $F^0() = \frac{\gamma}{2\pi}\int_0^{2\pi/\gamma} F().dt$

Then from [8], we have $a_{av}(t) - a(t) = \mathscr{O}(\varepsilon)$, and $\theta_{av}(t) - \theta(t) = \mathscr{O}(\varepsilon)$ on the time scale $1/\varepsilon$. After averaging F over the period $2\pi/\gamma$, and again with the approximation $2\gamma \approx \gamma + \omega$, we finally get the averaged equations as

$$\begin{aligned}\dot{a} &= -\frac{c_e(a)a}{2m} - \frac{1}{\gamma}\{\frac{\cos\theta}{2}[A + (B_1+B_2)\cos\alpha t] \\ &\quad + \frac{\sin\theta\sin\alpha t}{2}(B_2 - B_1)\} \\ \dot{\theta} &= \omega_e(a) - \omega + \frac{1}{a\gamma}\{\frac{\sin\theta}{2}[A + (B_1+B_2)\cos\alpha t] \\ &\quad - \frac{\cos\theta\sin\alpha t}{2}(B_2 - B_1)\}\end{aligned} \tag{16}$$

where ω_e and c_e are again given by (8) and (9). This corroborates the validity of REEP algorithm. Even with the multitone input, we see that the relationship between the equivalent parameters and sample properties (through $\overline{\Phi}_d$ and $\overline{\Phi}_c$) remain unchanged.

Simulations were done using piece-wise linear model ([2],[10]) of tip-sample interaction and cantilever was modeled as a second order system with $f_0 = 70kHz$ and $Q = 200$. Free air amplitude was chosen to be 24nm, and square pulses of 2nm and 1nm were given as sample. Equations (7) and (16) were solved simulataneously and difference in trajectories calculated via averaged equations and actual non-linear simulation is plotted in Fig.3. It was seen that the steady state error of multitone averaging equations have lesser error (around 60%) when compared to the monofrequency averaging equations.

III. Multimode Approximations

We saw that under the one-mode approximation, the approach for determining equivalent cantilever parameters necessitates the use of multi-frequency input. It is crucial to determine what is the effect of the input on additional modes and/or means of ascertaining extent of participation of the higher modes. There are attempts in the literature to address these operation modalities (see [11], [12] and the book [6]), however, as asserted in [6], the understanding on local material properties is scant. Also, to the best of the author's knowledge existing research has not leveraged averaging theory for facilitating determination of material properties in real-time particularly when multiple modes are involved. Taking the cue from the one-mode case, we develop an enabling paradigm that can elucidate the physics by evaluating whether an equivalent linear time-invariant system can be reached when multiple modes and multifrequency inputs are involved. We next present the challenges and approach toward this goal.

A. Challenges and Approach

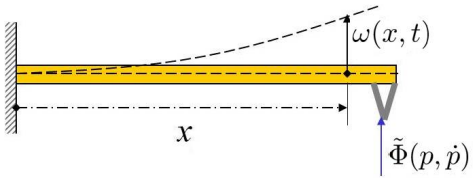

Fig. 4. An Euler-Bernoulli beam

In the dynamic mode, the cantilever tip interacts with the sample only intermittently. Thus it is intuitive that the mode shapes are mostly dictated by the fixed-free boundary conditions. The unforced Euler-Bernoulli beam (see Fig. 4) with one end fixed (at $x = 0$) and another end free (at $x = L$) is described by

$$\begin{aligned}&EI\frac{\partial^4 w(x,t)}{\partial x^4} + \rho A\frac{\partial^2 w(x,t)}{\partial t^2} = 0 \\ &w(0,t) = 0,\ \tfrac{\partial w(0,t)}{\partial x} = 0; \\ &EI\tfrac{\partial^2 w(L,t)}{\partial^2 x} = 0, EI\tfrac{\partial^3 w(L,t)}{\partial^3 x} = 0\end{aligned} \tag{17}$$

where $w(x,t)$ is the deformation at x and time t, with E, I, ρ, A representing appropriate cantilever properties.

We will assume that the natural mode shapes are described by $\psi_j(x)$. We will further assume that external excitation to the cantilever is provided as a forcing $\tilde{g} = \varepsilon g(t)$ at x_{exc} and the tip sample interaction forcing is given by $\tilde{\Phi}(p,\dot{p})$ at $x = L$ where $p(t) := w(L,t)$. Assuming an N mode approximation, it can be shown using variational principles (see [13]) that $w(x,t) = \sum_{i=1}^{N}\psi_j(x)q_j(t)$ where $q_j(t)$ satisfies

$$m_j\ddot{q}_j + \tilde{c}_j\dot{q}_j + k_j q_j = \tilde{g}_j(t) + \tilde{\Phi}_j(p,\dot{p}) \tag{18}$$

with $\tilde{g}_j(t) = \psi_j(x_{exc})\tilde{g}(t)$ and $\tilde{\Phi}_j(t) = \psi_j(L)\tilde{\Phi}(p,\dot{p})$. Let $g_j(t) = \psi_j(x_{exc})g(t)$ and $\Phi_j(t) = \psi_j(L)\Phi(p,\dot{p})$, then

$$\ddot{q}_j + \omega_j^2 q_j = \frac{\varepsilon}{m_j}(g_j(t) + \Phi_j(p,\dot{p}) - c_j\dot{q}_j) \tag{19}$$

where $\omega_j = \sqrt{k_j/m_j}$. Taking inspiration from the one-mode case we introduce new variables a_j and θ_j via

$$q_j = a_j \cos(\omega_j t + \theta_j), \quad \dot{q_j} = -a_j \omega_j \sin(\omega_j t + \theta_j). \tag{20}$$

The (a_j, θ_j) dynamics is given by

$$\begin{aligned} \frac{d}{dt}\begin{pmatrix} a_j \\ \theta_j \end{pmatrix} &= \varepsilon \begin{pmatrix} -\frac{f_j}{m_j \omega_j} \sin(\omega_j t + \theta_j) \\ -\frac{f_j}{m_j a_j \omega_j} \cos(\omega_j t + \theta_j) \end{pmatrix} \\ &=: \varepsilon \begin{pmatrix} h_{ja} \\ h_{j\theta} \end{pmatrix} =: \varepsilon \boldsymbol{h}_j(\boldsymbol{a}, \boldsymbol{\theta}, t) \end{aligned} \tag{21}$$

where $f_j = [g_j(t) + c_j a_j \omega_j \sin(\omega_j t + \theta_j) + \Phi_j(\sum_{j=1}^{\infty} a_j \cos(\omega_j t + \theta_j), \sum_{j=1}^{\infty} -a_j \omega_j \sin(\omega_j t + \theta_j))] =: f_j(\boldsymbol{a}, \boldsymbol{\theta}, t)$ with $\boldsymbol{a} := (a_1, \ldots, a_N)$ and $\boldsymbol{\theta} = (\theta_1, \ldots, \theta_N)'$. It is thus evident from (21), that the j^{th} amplitude a_j and phase θ_j dynamics are $O(\varepsilon)$. However, due to the presence of multiple modal frequencies, even if the excitation $\tilde{g}(t)$ is chosen to be periodic, $\boldsymbol{h} := (\boldsymbol{h}_1, \boldsymbol{h}_2, \ldots, \boldsymbol{h}_N)'$ will not be periodic in time t and thus the averaging theorem (Theorem II.1) cannot be applied. We will employ the notion of *generalized average* h^o of h defined via

$$\begin{aligned} \boldsymbol{h}^o(\boldsymbol{a}, \boldsymbol{\theta}) &= (\boldsymbol{h}_1^o, \boldsymbol{h}_2^o, \ldots, \boldsymbol{h}_N^o)', \text{ with} \\ \boldsymbol{h}_j^o(\boldsymbol{a}, \boldsymbol{\theta}) &= \lim_{T \to \infty} \frac{1}{T} \int_0^T \boldsymbol{h}_j(\boldsymbol{a}, \boldsymbol{\theta}, t) dt. \end{aligned} \tag{22}$$

It will also be important to determine how much the generalized average $\boldsymbol{h}^o$ differs from the time dependent $\boldsymbol{h}$ on a time scale $\frac{1}{\varepsilon}$. Here, we will use the measure

$$\delta(\varepsilon) := \sup_{(\boldsymbol{a}, \boldsymbol{\theta}) \in D} \sup_{t \in [0, L_t/\varepsilon]} \varepsilon \int_0^t [\boldsymbol{h}(\boldsymbol{a}, \boldsymbol{\theta}, \tau) - \boldsymbol{h}^o(\boldsymbol{a}, \boldsymbol{\theta})] d\tau \tag{23}$$

where D is some domain where we can determine that the amplitudes and phases remain in and L_t can be any strictly positive constant. With these definitions the following theorem holds [8].

Theorem III.1 (General First order averaging). *Consider*

$$\begin{aligned} \frac{d}{dt}\begin{pmatrix} a_j \\ \theta_j \end{pmatrix} &= \varepsilon \begin{pmatrix} h_{ja}(\boldsymbol{a}, \boldsymbol{\theta}, t) \\ h_{j\theta}(\boldsymbol{a}, \boldsymbol{\theta}, t) \end{pmatrix} \text{ and} \\ \frac{d}{dt}\begin{pmatrix} a_j \\ \theta_j \end{pmatrix}_{av} &= \varepsilon \begin{pmatrix} h_{ja}^o(\boldsymbol{a}_{av}, \boldsymbol{\theta}_{av}) \\ h_{j\theta}^o(\boldsymbol{a}_{av}, \boldsymbol{\theta}_{av}) \end{pmatrix} \end{aligned}$$

with the same initial conditions. Then on a time scale $\frac{1}{\varepsilon}$ the corresponding solutions differ at most by $O(\delta(\varepsilon))$.

The above result forms the analogue of Theorem II.1 for the time periodic case with the added onus of estimating the order of $\delta(\varepsilon)$ (for the periodic case $\delta(\varepsilon) = O(\varepsilon)$). Averaged equations for a_j and θ_j are obtained by evaluating $\boldsymbol{h}^o$ which results in (we have dropped the *av* subscript):

$$\begin{aligned} \dot{a_j} &= -\frac{c_{jeq}(\boldsymbol{a}, \boldsymbol{\theta}) a_j}{2m_j} \\ &\quad -\frac{1}{m_j \omega_j} \lim_{T \to \infty} \frac{\varepsilon}{T} \int_0^T g_j(t) \sin(\omega_j t + \theta_j) dt \\ \dot{\theta}_j &= \omega_{jeq}(\boldsymbol{a}, \boldsymbol{\theta}) - \omega_j \\ &\quad -\frac{1}{m_j a_j \omega_j} \lim_{T \to \infty} \frac{\varepsilon}{T} \int_0^T g_j(t) \cos(\omega_j t + \theta_j) dt \end{aligned} \tag{24}$$

where

$$\begin{aligned} \frac{c_{jeq}(\boldsymbol{a}, \boldsymbol{\theta})}{2m_j} &= \frac{\tilde{c}_j}{2m_j} + \frac{1}{a_j m_j \omega_j} \tilde{\Phi}_{jd} \text{ and} \\ \omega_{jeq}(\boldsymbol{a}, \boldsymbol{\theta})^2 &= \omega_j^2 - \frac{2}{a_j m_j} \tilde{\Phi}_{jc}, \text{ with} \end{aligned} \tag{25}$$

$$\begin{aligned} \tilde{\Phi}_{jd} &:= \lim_{T \to \infty} \frac{1}{T} \int_0^T \tilde{\Phi}_j(\sum_{j=1}^N a_j \cos(\omega_j t + \theta_j) \\ &\quad \sum_{j=1}^N -a_j \omega_j \sin(\omega_j t + \theta_j)) \sin(\omega_j t + \theta_j) dt \\ \tilde{\Phi}_{jc} &:= \lim_{T \to \infty} \frac{1}{T} \int_0^T \tilde{\Phi}_j(\sum_{j=1}^N a_j \cos(\omega_j t + \theta_j) \\ &\quad \sum_{j=1}^N -a_j \omega_j \sin(\omega_j t + \theta_j)) \cos(\omega_j t + \theta_j) dt \end{aligned}$$

The multi-mode averaged dynamics thus mirror the dynamics of the one mode case with $\tilde{\Phi}_{jd} = \tilde{\Phi}_{jd}(\boldsymbol{a}, \boldsymbol{\theta})$ and $\tilde{\Phi}_{jc} = \tilde{\Phi}_{jc}(\boldsymbol{a}, \boldsymbol{\theta})$ dependent on N amplitudes a_j and phase θ_j.

B. Energy Dissipation in each mode

Similar to the one mode case, it can be shown that the contribution to the sample dissipation power due to the deformation caused by the j^{th} mode of the cantilever, given by $\lim_{T \to \infty} -\frac{1}{T} \int_0^T \tilde{\Phi} \dot{q}_j dt$, is equal to $\lim_{T \to \infty} \frac{1}{T} \int_0^T (c_{jeq} - \tilde{c}_j) \dot{q}_j^2 dt$. Thus as was the case with the one mode approximation under the sample's influence the damping coefficient in the j^{th} mode can be considered as c_{jeq}, with the damping change caused by the sample in the j^{th} mode given by $c_{jeq} - \tilde{c}_j$. Again as in the one mode case if the sample is conservative, it can be shown that the total energy dissipation $\lim_{T \to \infty} -\sum_{j=1}^N \frac{1}{T} \int_0^T \tilde{\Phi} \dot{q}_j dt = 0$. In a similar manner the j^{th} resonant frequency due to sample interaction changes to ω_{jeq}. Thus the j^{th} mode dynamics are governed by $m_j \ddot{q}_j + c_{jeq} \dot{q}_j + k_{jeq} q_j = \tilde{g}_j$ and with the transfer function $\frac{1}{m_j s^2 + c_{jeq} s + k_{jeq}}$. Noting that $p(t) = \psi(L,t) = \sum_{j=1}^N \Psi_j(L) q_j(t)$ it follows that

$$\hat{p}(s) = \sum_{i=1}^N \frac{\psi_j(L) \hat{\tilde{g}}_j}{m_j s^2 + c_{jeq} s + k_{jeq}} \tag{26}$$

With the above development, assuming that the variables a_j and θ_j evolve on a slow time scale, the task is to identify a linear time invariant system of the form (26) from noisy measurement $y = p + v$. If the equivalent parameters k_{jeq} and c_{jeq} are determined, sample properties $\tilde{\Phi}_{jd}$ and $\tilde{\Phi}_{jc}$ can be evaluated. Summarizing the strategy for the multimode case consists of (a) arriving at an equivalent linear system (26) (b) estimating the coefficients of the linear system (26) via REEP (c) Obtaining the dissipative and the reactive power of the sample in the j^{th} mode (the weighted sum will provide the net dissipative and conservative (reactive) power).

C. Simulation results for multimode:

Simulations were performed in MATLAB on the same piece-wise linear model of tip-sample interaction and a two mode model of the AFM cantilever was considered. First mode has a resonant frequency $f_{01} = 70kHz$ with

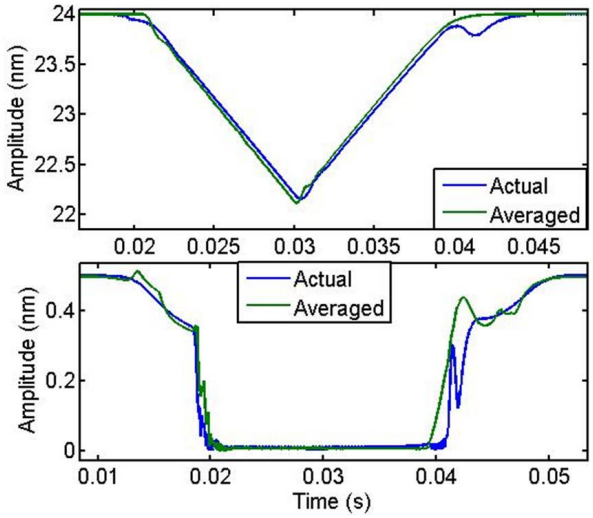

Fig. 5. Simulation results for the two-mode approximation of the cantilever dynamics compared with the averaged equations. (a) shows the amplitudes of the resonant frequency of the first mode, and (b) shows the amplitudes of the resonant frequency of the second mode.

quality factor $Q_1 = 200$ and the second mode has a resonant frequency $f_{02} = 6.3 \times f_{01}$ with quality factor $Q_2 = 1000$ (these are the typical parameters of the Olympus AC240TS cantilever). Cantilever was excited with a sum of two sinusoids (the first and second modal frequencies) such that with no sample interaction, the magnitude of the cantilever deflection at the first modal frequency (termed as the amplitude at the first mode) was $24nm$. Similarly the amplitude at the second mode was $0.5nm$. Amplitudes for both modes were calculated by demodulating the cantilever trajectory of the non-autonomous system of (18) at the two resonant frequencies. Averaging equation (24) for the two modes was considered and was solved in MATLAB using the same non-linear tip-sample interaction model. Infinite integral in (24) was suitably approximated with a finite T during the simulation. Amplitudes calculated for both modes were compared to the ones calculated via solving the actual dynamical equations. Figure 5 shows the simulation results where the sample is slowly raised ($2nm$) towards the cantilever tip (in the approach phase) till 0.03 seconds and then retracted away from the sample (in the retract phase). The amplitudes at the first mode and second mode are then compared with the averaged equations. We see that the averaged dynamics do indeed match the real amplitudes well. This provides evidence that averaging theory based results can be used and thus directs the future research to the determination of equivalent parameters and subsequently the sample dissipation and reactive power at higher modes.

IV. Conclusion and Future Directions

In this paper, we have arrived at a means of modeling the non-linear tip-sample interaction as an equivalent linear system when excitation is a sum of sinusoids. It was shown that the local dissipation and stiffness properties can be calculated by estimating the parameters of the second order (first mode) equivalent cantilever model of the cantilever. The real utility of methods proposed is the ability of *simultaneous* determination of the *local stiffness* of the sample and the local dissipation. We further extended the equivalent cantilever paradigm to the multi-mode model of the cantilever and showed simulation results supporting the model in the case of two-mode approximation. The paradigm laid out is quite general with a potential for wide applicability. Pertinent questions include, what kind of materials is it beneficial to involve higher modes and multi-frequency excitation; when do the estimates on dissipation and stiffness remain meaningful; are there alternate forms of representing averaged dynamics under which the error from the original remain small. We have provided directions based on averaging theory to address such questions. In future work, we will focus on the piece-wise linear model of the tip-sample interaction and will include multiple mode approximation of the cantilever under which we will address the issues outlined above.

References

[1] D. Pires, J. Hedrick, A. De Silva, J. Frommer, B. Gotsmann, H. Wolf, M. Despont, U. Duerig, and A. Knoll, "Nanoscale Three-Dimensional Patterning of Molecular Resists by Scanning Probes," *Science*, vol. 328, no. 5979, p. 732, 2010.

[2] A. Sebastian, M. V. Salapaka, D. J. Chen, and J. P. Cleveland, "Harmonic analysis based modeling of tapping-mode afm," *Proceedings of the American Control Conference*, pp. 232–236, June 1999.

[3] P. Agarwal and M. Salapaka, "Real time estimation of equivalent cantilever parameters in tapping mode atomic force microscopy," *Applied Physics Letters*, vol. 95, no. 8, p. 083113, 2009.

[4] D. R. Sahoo, A. Sebastian, , and M. V. Salapaka, "Harnessing the transient signals in atomic force microscopy," *International Journal of Robust and Nonlinear Control*, vol. 15, pp. 805–820, 2005.

[5] J. Melcher, C. Carrasco, X. Xu, J. Carrascosa, J. Gómez-Herrero, P. José de Pablo, and A. Raman, "Origins of phase contrast in the atomic force microscope in liquids," *Proceedings of the National Academy of Sciences*, vol. 106, no. 33, p. 13655, 2009.

[6] R. García, *Amplitude Modulation Atomic Force Microscopy*. Wiley-VCH, 2010.

[7] N. N. Bogoliubov and Y. A. Mitropolskii, *Asymptotic methods in the theory of non-linear oscillations*. New Delhi, India: Hindustan publishing corporation, 1961.

[8] J. Sanders, F. Verhulst, and J. Murdock, *Averaging methods in nonlinear dynamical systems*. Springer Verlag, 2007.

[9] J. Cleveland, B. Anczykowski, A. Schmid, and V. Elings, "Energy dissipation in tapping-mode atomic force microscopy," *Applied Physics Letters*, vol. 72, p. 2613, 1998.

[10] A. Sebastian, M. V. Salapaka, D. Chen, and J. P. Cleveland, "Harmonic and power balance tools for tapping-mode atomic force microscope," *Journal of Applied Physics*, vol. 89 (11), pp. 6473–6480, June 2001.

[11] R. W. Stark, "Dynamics of repulsive dual-frequency atomic force microscopy," *Applied Physics Letters*, vol. 94, no. 6, pp. 063 109 – 063 109–3, feb 2009.

[12] J. R. Lozano and R. Garcia, "Theory of multifrequency atomic force microscopy," *Phys. Rev. Lett.*, vol. 100, p. 076102, Feb 2008. [Online]. Available: http://link.aps.org/doi/10.1103/PhysRevLett.100.076102

[13] M. V. Salapaka, H. S. Bergh, J. Lai, A. Majumdar, and E. McFarland, "Multi-mode noise analysis of cantilevers for scanning probe microscopy," *Journal of Applied Physics*, vol. vol. 81(6), pp. 2480–2487, March 1997.